

Optimal transseptal puncture location for robot-assisted left atrial catheter ablation

J. Jayender^{1,4*}

R. V. Patel²

G. F. Michaud³

N. Hata¹

¹*Surgical Planning Laboratory,
Department of Radiology, Harvard
Medical School, Brigham and
Women's Hospital, Boston, MA, USA*

²*Department of Electrical and
Computer Engineering and
Department of Surgery, University of
Western Ontario, Canadian Surgical
Technologies and Advanced Robotics
(CSTAR), London, ON, Canada*

³*Department of Cardiology, Harvard
Medical School, Brigham and
Women's Hospital, Boston, MA, USA*

⁴*Clinical Image Guidance Laboratory,
Center for Center for Integration of
Medicine, and Innovative Technology,
Massachusetts General Hospital,
Boston, MA, USA*

*Correspondence to: J. Jayender,
Surgical Planning Laboratory,
Department of Radiology, Harvard
Medical School, Brigham and
Women's Hospital, Boston, MA
02115, USA. E-mail:
jayender@bwh.harvard.edu

Abstract

Background The preferred method of treatment for atrial fibrillation (AF) is by catheter ablation, in which a catheter is guided into the left atrium through a transseptal puncture. However, the transseptal puncture constrains the catheter, thereby limiting its manoeuvrability and increasing the difficulty in reaching various locations in the left atrium. In this paper, we address the problem of choosing the optimal transseptal puncture location for performing cardiac ablation to obtain maximum manoeuvrability of the catheter.

Methods We have employed an optimization algorithm to maximize the global isotropy index (GII) to evaluate the optimal transseptal puncture location. As part of this algorithm, a novel kinematic model for the catheter has been developed, based on a continuum robot model. Pre-operative MR/CT images of the heart are segmented using the open source image-guided therapy software, 3D Slicer, to obtain models of the left atrium and septal wall. These models are input to the optimization algorithm to evaluate the optimal transseptal puncture location.

Results The continuum robot model accurately describes the kinematics of the catheter. Simulation and experimental results for the optimal transseptal puncture location are presented in this paper. The optimization algorithm generates discrete points on the septal wall for which the dexterity of the catheter in the left atrium is maximum, corresponding to a GII of 0.4362.

Conclusion We have developed an optimization algorithm based on the GII to evaluate the optimal position of the transseptal puncture for left atrial cardiac ablation. Copyright © 2011 John Wiley & Sons, Ltd.

Keywords cardiac ablation; continuum robot; optimal port; robot-assisted; global isotropy index

Introduction

Atrial fibrillation (AF) is a type of arrhythmia where the atria beat irregularly and out of coordination with the ventricles. When rate and rhythm control drugs are ineffective in patients suffering from AF, catheter ablation is performed as a standard method of treatment. In this procedure, a steerable sheath is first guided through the femoral vein into the right atrium under biplane X-ray uoroscopy and transoesophageal echocardiography (TEE) or intracardiac echocardiography (ICE). A transseptal puncture is then created in the interatrial septal wall, using a needle which is passed through the steerable sheath. The ablation catheter is then guided to the left atrium through the steerable sheath, which is pivoted about the transseptal puncture location. In

Accepted: 25 February 2011

turn, the ablation catheter is also constrained at this point. Once the catheter makes contact with the abnormal electrical pathways creating arrhythmia, radiofrequency energy (or cryoenergy) is delivered to these points to create necrosis and restore normal sinus rhythm.

More recently, a robotics based master–slave approach for performing cardiac ablation has been introduced. Several research groups have studied the problem of employing a master–slave robotic system to aid in the insertion of a catheter. The most notable work was by Fukuda *et al.* (1–3) and Jayender *et al.* (4–6). Two companies, Hansen Medical and Stereotaxis, have developed robotic systems to perform cardiac ablation. At our institution, we have direct clinical experience with the Sensei robot from Hansen Medical (7). Although the robot is capable of precise catheter motions and maintaining stable contact with the heart wall, the clinician often encounters difficulty in manoeuvring the catheter and approaching the desired point on the heart at the required angle. The lack of dexterity of the catheter arises from the constraint imposed on the motion of the catheter due to the transseptal puncture (8) (see Figure 1). The interatrial septal wall effectively acts like a remote centre of motion (RCM), about which the catheter is manipulated. This can severely affect the dexterity and manoeuvrability of the catheter, thereby affecting the clinician's performance. In addition, there is also danger of perforating the aortic arch with catastrophic results, due to accidental needle puncture (9). Therefore, it is of prime importance for the clinician to puncture the transseptal wall at an optimal point to maximize the dexterity of the catheter in the left atrium while minimizing the possibility of puncturing the aortic arch. In this paper, we develop a computational algorithm to determine the optimal transseptal puncture location for performing cardiac ablation. Once determined, the puncture location will be registered to the intracardiac echo (ICE) image, so that the clinician can guide the needle in real time to the optimal puncture location to obtain maximum manoeuvrability of the catheter, while avoiding puncturing of the aorta.

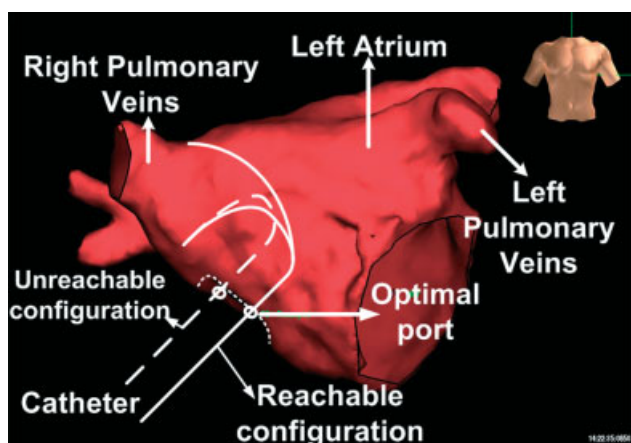


Figure 1. Difficulty in manoeuvring the catheter due to improper transseptal puncture location

In this paper we have adopted the global isotropy index (GII) (10,11) to define the performance measure for quantifying the dexterity of the catheter within the left atrium. We have developed an optimization algorithm to maximize the GII for efficiently manoeuvring the catheter in the left atrium. In order to develop the algorithm, the first step is to model the catheter.

There has been quite a bit of interest in developing models and control techniques for exible, hyper-redundant and underactuated robots, such as a robotic catheter. Hyper-redundant robots have a large or infinite number of degrees of kinematic redundancy (12). Several control techniques have been proposed for such systems (13–16). Another class of manipulators, called continuum robots, have also gathered a lot of interest recently in modelling systems such as catheters. Continuum robots do not have rigid links; instead the manipulators bend continuously along their length and generate smooth curves (17). Some research has also utilized the model for continuum robots to model catheters, e.g. in (18) a continuum robot model has been used to model an active catheter instrumented with pressure bellows along the manipulator; in (19) a continuum robot model has been used to model the distal end of a cardiac ablation catheter. It should be noted that in both of these papers the continuum robot falls under the intrinsic category wherein the actuators lie along the length of the manipulator. In order to model the catheter, we adopt the algorithm developed by Mochiyama and Suzuki (20) and Tatlicioglu *et al.* (21). However, we have extended the modelling of the catheter to a more general framework by including bending of the catheter in both possible directions and also allowing for the extensibility of the catheter. We only consider the segment of the catheter inside the left atrium of the heart.

To the best of our knowledge, this is the first study that addresses the issue of evaluating the optimal transseptal puncture location for performing left atrial cardiac ablation. In addition, we have also contributed to the robotics literature by generalizing the continuum robot model for the two-dimensional (2D) bending motion with extensibility of the catheter. The development of such an algorithm will significantly improve the dexterity of the catheter within the left atrium and thereby may minimize the duration of the procedure from an average of 4 h, minimize the amount of energy and lesions required to isolate the pulmonary veins and reduce the amount of fatigue for the clinician. In addition, the choice of the transseptal puncture will also ensure that the robot is away from any singularity while accessing all locations in the left atrium.

Methods

Modelling of catheter

The catheter is considered as being made up of infinitesimal rigid links along a backbone curve. The

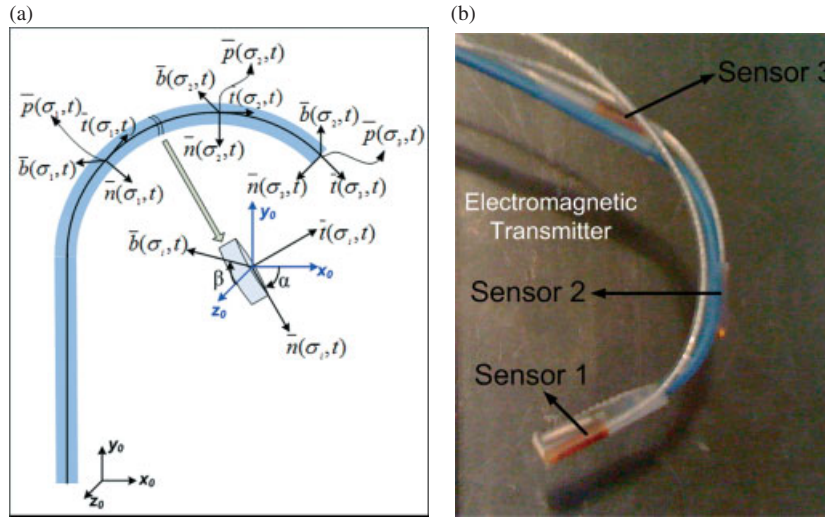


Figure 2. (a) Model for the catheter; (b) experimental set-up

backbone curve is defined in terms of the Frenet–Serret frame. The curve is represented in the parametric form, $\bar{x} = \bar{x}(\sigma, t)$, where σ is the parameter which represents the curve length and t is the time. The Frenet–Serret frame is defined at each point $p(\sigma, t)$ along the backbone curve and consists of the tangent $\bar{t}(\sigma, t)$, normal $\bar{n}(\sigma, t)$ and binormal $\bar{b}(\sigma, t)$ vector at point $p(\sigma, t)$, as shown in Figure 2a. At any point $p(\sigma, t)$ along the curve $\bar{x}(\sigma, t)$, the local frame can be defined as ${}^0\Phi(\sigma, t)$. In terms of the Euler angles, the frame ${}^0\Phi(\sigma, t)$ can be defined with respect to the base frame ${}^0\Phi(0, t)$ as a rotation of α about $\bar{b}(\sigma)$ and β about $\bar{n}(\sigma)$ vector. Also, the angles α and β can be defined in terms of the curvature and torsion as follows:

$$\alpha = \int_0^\sigma \zeta(v, t) dv \quad \beta = \int_0^\sigma \tau(v, t) dv \quad (1)$$

In this case, we assume that the curvature ζ and torsion τ are constant. Therefore, ${}^0\Phi(\sigma, t)$ can be written as:

$${}^0\Phi(\sigma, t) = \text{Rot}(\bar{b}, \alpha)\text{Rot}(\bar{n}, \beta) \text{ i.e.,} \quad (2)$$

that is:

$${}^0\Phi(\sigma) = \begin{bmatrix} \cos(\sigma\zeta) \cos(\sigma\tau) & -\sin(\sigma\zeta) \cos(\sigma\zeta) \sin(\sigma\tau) \\ \sin(\sigma\zeta) \cos(\sigma\tau) & \cos(\sigma\zeta) \sin(\sigma\zeta) \sin(\sigma\tau) \\ -\sin(\sigma\tau) & 0 & \cos(\sigma\tau) \end{bmatrix} \quad (3)$$

The position vector $\bar{p}(\sigma, t)$ of a point on the curve relative to the origin $\bar{p}(0)$ can be computed by integrating infinitesimal curve lengths along the tangent vector. In other words, ${}^0\bar{p}(\sigma)$, as viewed in the base frame ${}^0\Phi(0)$ is given by:

$${}^0\bar{p}(\sigma, t) = \int_0^\sigma {}^0\Phi(\eta, t) \hat{e}_x d\eta \quad (4)$$

where $e_x := [1 \ 0 \ 0]^T$. Each segment of the catheter within the heart can be considered to consist of two rotational

joints and a prismatic joint. The joint angle vector can be written as $\bar{\theta} = [0 \ \zeta \ \tau]^t$ and the translational vector can be written as $\bar{d} = [l_x \ 0 \ 0]^t$, where l_x is the extension of the length of the catheter. The rotational velocity for a joint in the local Frenet–Serret frame with respect to the base frame can be written as:

$${}^0\omega(\sigma) = \int_0^\sigma \bar{\theta}^\sigma \Phi(v) dv \text{ (for a rotational joint)} \quad (5)$$

$${}^0\omega(\sigma) = 0 \text{ (for a prismatic joint)} \quad (6)$$

Similarly, the translational velocities for the rotational and prismatic joints can be written as:

$${}^0v(\sigma) = \int_0^\sigma \bar{\theta}^\sigma \Phi(v) \times ({}^\sigma p(v, t) - {}^\sigma p(0, t)) dv \text{ (for a rotational joint)} \quad (7)$$

$${}^0v(\sigma) = \int_0^\sigma \bar{d}^\sigma \Phi(v) dv \text{ (for a prismatic joint)} \quad (8)$$

Equations (5–8) together can be written in a compact form as:

$$\begin{bmatrix} {}^0v(\sigma) \\ {}^0\omega(\sigma) \end{bmatrix} = \int_0^\sigma \begin{bmatrix} {}^\sigma\Phi(v, t) & [p(v, t) - p(0, t) \times] \Phi(v, t) \\ 0 & \Phi(v, t) \end{bmatrix} \bar{A} \begin{bmatrix} \dot{d} \\ \dot{\zeta} \\ \dot{\tau} \end{bmatrix} dv \quad (9)$$

where:

$$\bar{A} = \begin{bmatrix} 1 & 0 & 0 & 0 & 0 & 0 \\ 0 & 0 & 0 & 0 & 0 & 1 \\ 0 & 0 & 0 & 0 & 1 & 0 \end{bmatrix}^T$$

$$\text{and } [a \times] \triangleq \begin{bmatrix} 0 & -a_z & a_y \\ a_z & 0 & -a_x \\ -a_y & a_x & 0 \end{bmatrix} \quad (10)$$

Using the standard robotics terminology, the Jacobian operator can be defined as:

$$\mathcal{J}(\sigma, t) = \int_0^\sigma \begin{bmatrix} {}^\sigma\Phi(v, t) & [p(v, t) - p(\sigma, t) \times] \Phi(v, t) \\ 0 & \Phi(v, t) \end{bmatrix} \bar{A}(\cdot) dv \quad (11)$$

From equation (4), we can estimate the position of the catheter with respect to the base coordinates for a given configuration of the catheter. However, for the optimization algorithm, we will assume that the catheter is in contact with a certain point inside the left atrium while being constrained at the transseptal puncture location. Therefore, this gives us the base and end-effector coordinates of the catheter. It is required to solve the inverse kinematics problem to evaluate the configuration of the catheter for the distal end of the catheter to be in contact with a particular point inside the heart. The problem of solving the inverse kinematics of the catheter is formulated as a dynamical problem, which requires only the computation of the forward kinematics, as determined by equation (4). The joint variable, represented as $q(t) \in \mathfrak{R}^3$, is defined as:

$$q = [l_x \ \varsigma \ \tau]^T$$

Let us represent the solution of the inverse kinematics problem as $\hat{q}(t)$ corresponding to a trajectory $\hat{x}(t)$, which satisfies the forward kinematics given by equation (4). Let $e(t)$ represent the error between the desired Cartesian position $\hat{x}(t)$ and the actual Cartesian position obtained from the state variable q of the iteration algorithm. The error dynamics can be written as:

$$\dot{e}(t) = \dot{\hat{x}}(t) - \dot{x}(t) = \dot{\hat{x}}(t) - \mathcal{J}\dot{q} \quad (12)$$

We choose a purely proportional control law to solve for \dot{q} as given by:

$$\dot{q} = \alpha \mathcal{J}^T e \quad (13)$$

It has been shown [22] that by choosing a control law as given by equation (13), the error e is bounded and can be made small with an appropriate choice of α , with the added benefit of less computational complexity. Therefore, the algorithm consists of the following steps:

- Choose the initial value of q_0 .
- Begin Loop:
- From forward kinematics, compute the Cartesian position x_k for corresponding joint variable q_k
- Calculate the error vector $e_k = \hat{x} - x_k$
- If $e_k < \text{tol}(= 1e^{-12})$, exit loop
- Calculate $q_{k+1} = q_k + \alpha \mathcal{J}^T e$
- Go to Begin Loop
- End Loop
- Inverse kinematics solution is q_n

Global isotropy index

The Jacobian matrix relates the end-effector frame velocities \dot{x} and forces f to the corresponding joint rates \dot{q} and torques τ , as given by the following equations:

$$\dot{x} = \mathcal{J}\dot{q} \quad (14)$$

$$\tau = \mathcal{J}^T f \quad (15)$$

Condition number κ of the Jacobian \mathcal{J} can be considered as the error amplification factor from the joint space to the Cartesian space. Taking the norm on both sides of equation (14), we obtain:

$$\frac{\|\delta x\|}{\|x\|} \leq \|\mathcal{J}^{-1}\| \frac{\|\delta q\|}{\|q\|} \quad (16)$$

The condition number κ is, therefore, defined [23] as:

$$\kappa(\mathcal{J}) = \|\mathcal{J}^{-1}\| \|\mathcal{J}\| = \frac{\bar{\sigma}(\mathcal{J}(q))}{\underline{\sigma}(\mathcal{J}(q))} \quad (17)$$

where $\bar{\sigma}$ and $\underline{\sigma}$ represent the maximum and minimum singular values of \mathcal{J} . The condition number represents the dexterity of the robot at a specified point, and often the inverse of the condition number is used, since the value of $\kappa(\mathcal{J})^{-1} \in [0, 1]$. For a robot in a singular configuration, $\underline{\sigma} = 0$, implying that for $\kappa(\mathcal{J})^{-1} = 0$. The closer $\kappa(\mathcal{J})^{-1}$ or $\kappa(\mathcal{J})$ is to unity, the more accurate and dextrous the robot is. A configuration of the robot is defined as an isotropic configuration, which is the most dextrous configuration for the robot, when the condition number $\kappa(\mathcal{J})$ corresponding to this configuration is unity. Therefore, in order to ensure that the robot (in our case the catheter) is well controlled in all regions of the left atrium, we try to maximize the dexterity or a measure of isotropy. However, it should be noted that the Jacobian is a function of the local position (in turn joint variables), therefore the condition number is a local measure of the dexterity of the robot at any position. The transseptal puncture location should be chosen such that the dexterity of the catheter is maximized at all points in the left atrium. Therefore, there is a need to define the performance measure as a global measure rather than a local measure. In (10), the GII was proposed to define the overall dexterity of the robot throughout the workspace. The GII is defined as:

$$GII(y_i) = \frac{\min_{x_0 \in W_i} \underline{\sigma}(\mathcal{J}(x_0))}{\max_{x_1 \in W_i} \bar{\sigma}(\mathcal{J}(x_1))} \quad (18)$$

where $W_i = W(y_i) = \{x_k - y_i : x_k \in W_a\}$, $y_i \in W_s$. For our application, $W_a \in \mathfrak{R}^3$ is the set of points on the left atrium and $W_s \in \mathfrak{R}^3$ is the set of points on the septal wall. It should be noted that GII is a global measure, as compared to the condition number, which is a local measure. It should also be noted that the GII is related to the inverse of the condition number, rather than the condition number itself, in order to restrict the values to the range [0, 1]. A

GII of 1 implies that the catheter is isotropic at every point in the workspace and behaves uniformly in all directions, which is the ideal condition.

Since linear and circumferential lesions may be needed at most points in the left atrium, depending on the type of atrial fibrillation (persistent, paroxysmal or permanent), we consider the surgical workspace to be the entire left atrium. The workspace can be further reduced, based on the clinician's input in the pre-operative stage. The problem is to choose the transeptal puncture location to maximize the dexterity of the catheter while accessing the surgical workspace. The dexterity of the catheter in the surgical workspace is quantified in terms of the GII. The optimization algorithm searches for the point $y_{opt} \in W_s$, which maximizes the GII, corresponding to the optimal location for the transeptal puncture. This location constrains the catheter and can be considered as the base coordinates of the catheter. The distal end of the catheter (considered as the end-effector) touches the points on the left atrium. For each point on the left atrium, the configuration of the catheter is estimated using inverse kinematics and the corresponding Jacobian \mathcal{J} and singular values ($\bar{\sigma}$, $\underline{\sigma}$) are evaluated and provided to the optimization algorithm.

Segmentation of left atrium and septal wall

The point sets W_a and W_s , representing the data points on the left atrium and septal wall, respectively, are obtained by segmenting the heart from a pre-operative CT/MR image. In our experiments, we have employed the open

source, image-guided therapy software, 3D Slicer (24), to load and segment the cardiac MR images. Slicer is an open-source software which is compatible with several platforms and is specifically designed to visualize and analyse medical image data. In addition, the software is also equipped with modules to perform manipulations and computations on medical images, in addition to executing standard image-processing algorithms. The user manually segments the left atrium, right atrium and septal wall from each slice of the pre-operative MR/CT images in Slicer.

Once the segmentation is complete, a three-dimensional (3D) model is created. The VTK files of the left atrium and the septal wall corresponding to the models are then input to the optimization algorithm. A snapshot of the models created in Slicer with a single slice view is shown in Figure 3.

Results

Graphical validation of model

The objective of this experiment was to simulate the model for the catheter and visually validate it for any singularities in the workspace. The hypothesis was that, in the absence of any singularities, the simulated model would show a uniform increase in curvatures and extension upon actuation. The kinematic equations (4), (12) and (13) were implemented as vtk classes. The coordinates of 20 points along the catheter have been computed and displayed as a spline around which a tube has been created, using the vtkTubeFilter class. The distal tip of the catheter is controlled by means of a haptic device,

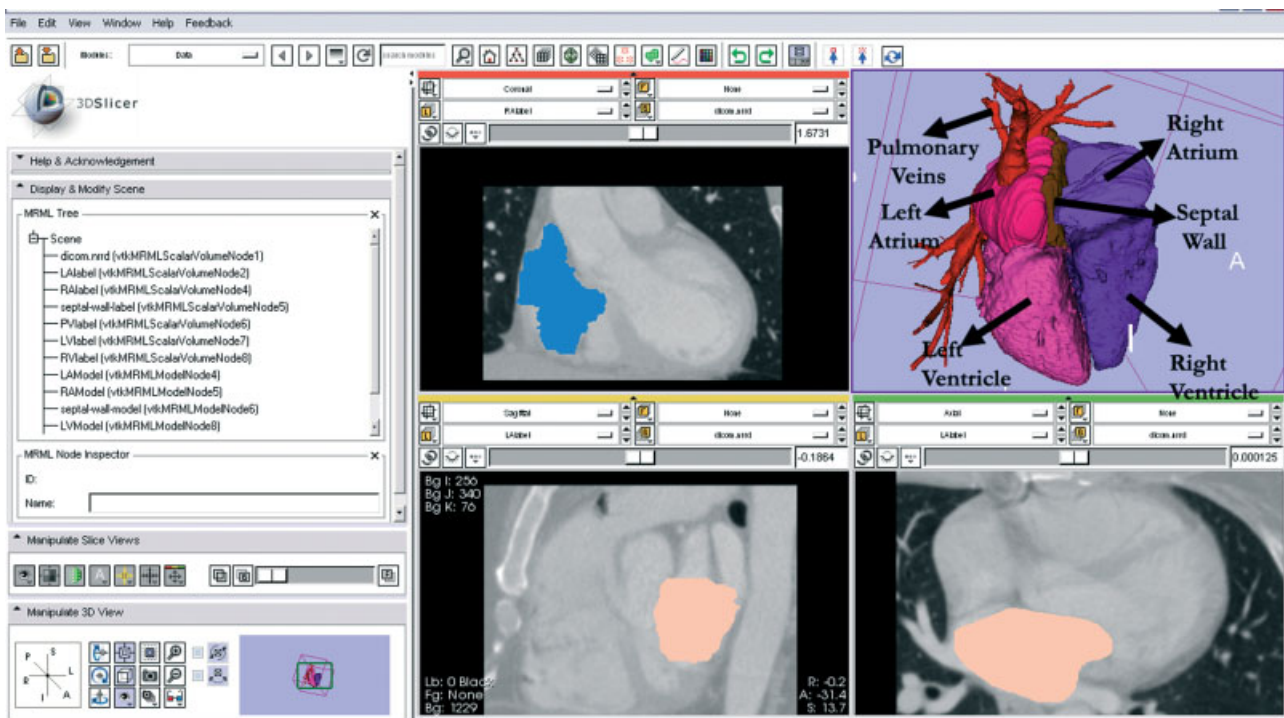


Figure 3. Slicer interface

which is interfaced to Slicer using the OpenIGTLink. The OpenIGTLink (25) is a network protocol that enables the transfer of various data types among different hardware (such as MRI scanners, robotic devices, tracking devices, etc.) and software modules (other modules in 3D Slicer, simulink models in MATLAB, etc.). In our case, the haptic device was controlled using an Intel Centrino Laptop running at 1.7 GHz with 2 GB RAM. The laptop was connected to an Intel Quad-Core Xeon computer running at 3.4 GHz with 32 GB RAM on which Slicer was loaded. The Cartesian coordinates of the distal end of the catheter were directly controlled by the haptic device. It should be noted here that the haptic device was used only a master device to provide the desired trajectory to the catheter, while no force feedback was enabled. The configuration of the catheter ($s_{distal}, \zeta_{distal}, \tau_{distal}$) was computed using the inverse kinematics, as defined by equations (12) and (13). The coordinates of the remaining points on the catheter were computed at equidistant points along the catheter ($s_i = i \cdot s_{distal} = 20$ for $i = 1, 2 \dots 19$) while maintaining the same curvature ($\zeta_{distal}, \tau_{distal}$) along the catheter, using the forward kinematics defined by equation (4). The results are shown in Figure 4.

Experimental validation of model

The objective of this experiment was to experimentally validate the continuum robot model. Three electromagnetic position sensors (6-DOF Microbird, Ascension Technologies (ATC), Burlington, VA, USA) were placed at three locations on the catheter (see Figure 2b). Sensor 1 was placed at the distal end of an ablation catheter (St. Jude Medical Inc.), while sensor 2 was placed 3.3 cm from the distal sensor in the curved section of the catheter, and sensor 3 was placed 9.2 cm from sensor 1. The ATC electromagnetic system was connected to an Intel Quad Core 2 GHz computer with 4 GB RAM. The position readings were logged at a sampling rate of 67 Hz, using MATLAB Simulink. The catheter was manually actuated to execute a trajectory. Since sensor 3 was placed at the non-bending section of the catheter, it was considered as the base coordinates of the continuum robot, while sensor 1, placed at the distal tip of the catheter, was considered as the end-effector coordinates of the robot. At each time point, the inverse kinematics were solved to obtain the configuration of the catheter (s, ζ, τ). The position of sensor

2 was estimated by forward kinematics, considering the joint coordinates of sensor 2 as $(d_{23}/d_{13}s, \zeta, \tau)$, where d_{ij} is the distance of sensor i from sensor j . The RMS error of the position of sensor 2 estimated from forward kinematics and the measured position of the sensor was 6.7 mm.

Clinical validation

The objective of this experiment was to correlate the difficulty of manipulating the catheter with the GII for the specific region of interest. In this test, we segmented the left atrium and the pulmonary veins of a male patient suffering from atrial fibrillation who was treated at the Brigham and Women's Hospital, Boston, MA. The segmentation and 3D model generation were performed on contrast-enhanced magnetic resonance (MR)-angiography images obtained from a 3.0T Siemens MRI scanner. The series consisted of 56 slices, with resolution of $0.4 \times 0.4 \times 0.7$ mm. The study was carried out post-procedurally. The ablation procedure was performed by first inserting a steerable sheath through a transseptal puncture, which was created under intracardiac echo (ICE) imaging and biplane fluoroscopy. It should be noted here that the clinician punctured the septal wall at a position considered to be ideal but not computed using the algorithm developed in this paper. A St. Jude Medical ablation catheter was then introduced into the left atrium through the steerable sheath. The left atrium was mapped using the NavX Ensite system from St. Jude Medical Inc. At the end of the procedure, the steerable sheath was gradually dragged back on the septal wall to register the point of transseptal puncture, using the Ensite system. The data points were exported from the Ensite system to 3D Slicer, which was further registered to the 3D models generated from pre-operative MR images. The VTK file corresponding to the left atrium was input to the optimization algorithm along with the transseptal puncture coordinates. The expert clinician was also given the task of delineating the areas which were difficult to navigate during the procedure. The region marked was around the septal wall and the right pulmonary veins.

In the first case, the entire left atrium was chosen as the desired workspace for the ablation catheter. The GII corresponding to the transseptal puncture location was calculated to be 0.0570. Since the transseptal puncture

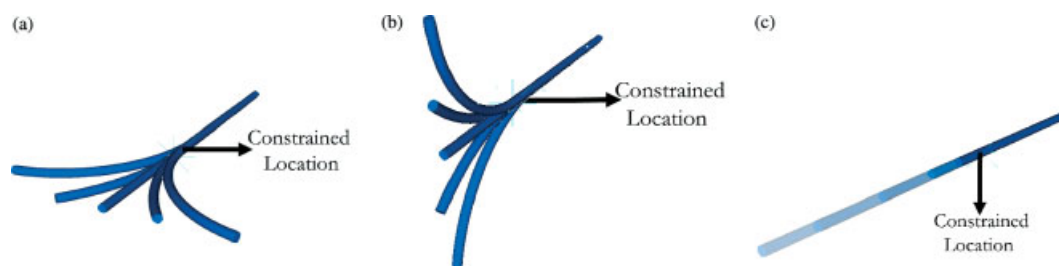


Figure 4. (a) Catheter configuration showing a smooth increase in curvature κ ; (b) catheter configuration showing a smooth increase in curvature τ ; (c) catheter configuration showing a smooth increase in its length

point was not chosen to correspond to the optimal port, the GII value corresponding to this point is considerably low. Further, the regions delineated by the clinician were provided to the algorithm to compute the GII only in this region. The GII corresponding to the region around the septal wall was obtained as 0.0051, while that corresponding to the right pulmonary region was 0.0055.

GII optimization

A pre-operative CT image was first loaded in 3D Slicer. The CT image was a contrast enhanced image consisting of 64 slices. The resolution of each slice was $0.7 \times 0.7 \times 0.7$ mm. An expert radiologist was given the task of manually segmenting the left atrium, the septal wall and the right atrium. The models were then generated in 3D Slicer and the corresponding VTK file, consisting of the data points of the model, was created. The file consisting of the coordinates of the left atrium and the septal wall were input to the optimization algorithm. The optimal transseptal puncture location algorithm was implemented using MATLAB on an Intel Core2 Duo 2.00 GHz machine with 1 GB RAM. Figure 5a, b shows the results of the variation of GII as a function of the

x and y coordinates, respectively. The maximum value of GII was 0.4362, a location which provides the best isotropy and in turn dexterity of the catheter. In addition, the GII values were converted to a scalar VIBGYOR colour map (red representing low GII and violet representing high GII), corresponding to the points in the VTK file and displayed on the model of the septal wall in Slicer, as shown in Figure 6a. The mean value of GII on the septal wall was 0.0327. Figure 6b shows the location of the optimal puncture with respect to the left and right atria. Figure 7a shows the mesh plot of the GII on the septal wall. The colour bar reflects the values of the GII at different locations on the septal wall. In Figure 7(b), we have compared the condition number κ for six points on the left atrium, corresponding to two transseptal puncture locations, S_1 and S_2 .

Discussion

In this paper, we have developed a model for the catheter in the left atrium. We have extended the modelling of the catheter to a more general framework by including bending of the catheter in both possible directions and also

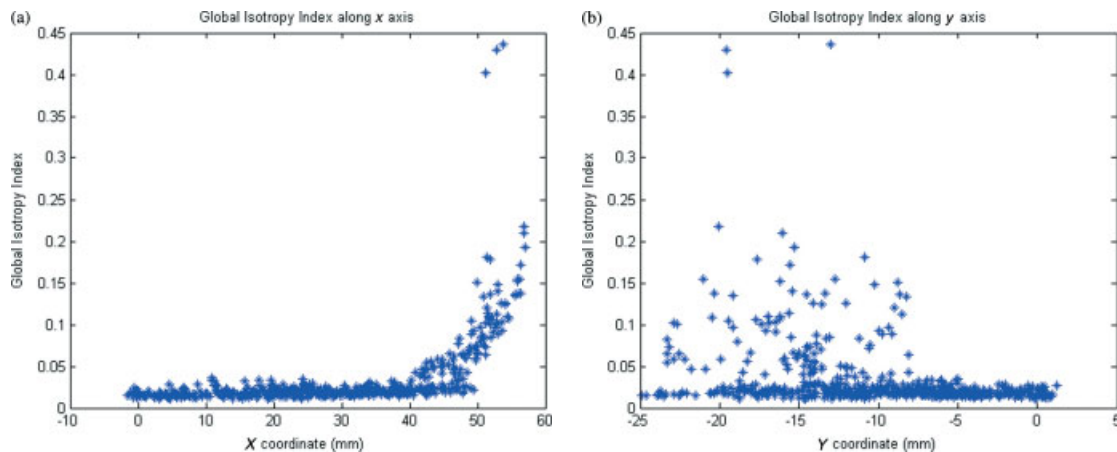


Figure 5. (a) Graph showing the variation of GII as a function of the x coordinate; (b) graph showing the variation of GII as a function of the y coordinate

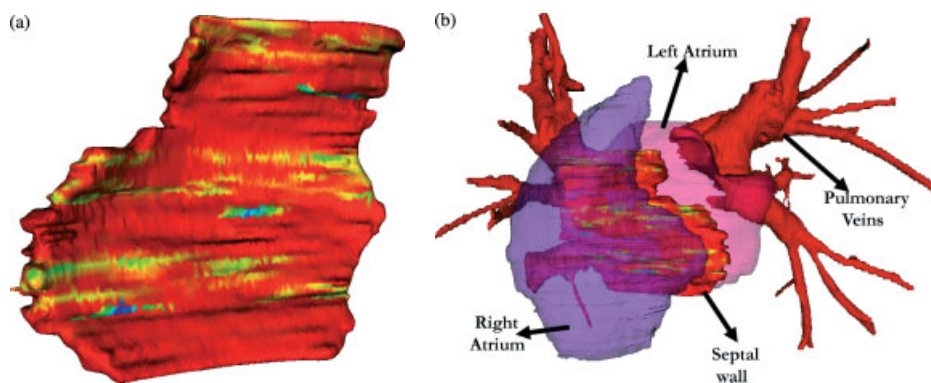


Figure 6. (a) Magnified view of the septal wall with the VIBGYOR colour map, representing the GII at various locations. Red represents points with low GII, while blue represents points with high GII; (b) segmented model of the LA, RA, PV and septal wall, with the colour map representing the GII at different locations

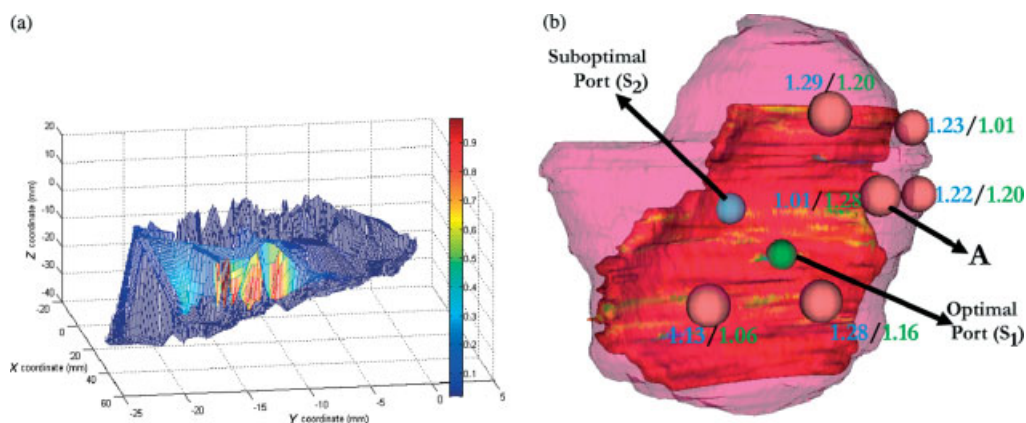


Figure 7. (a) Mesh plot showing the colour map overlaid over the septal wall with colour bar representing the GII; (b) 3D view of two points chosen on the septal wall and six points on the LA. The condition number corresponding to each point is represented as x_2/x_1 , where x_2 corresponds to the condition number of the point, assuming that the catheter is passing through the suboptimal port S_2 , and x_1 corresponds to the condition number of the point, assuming that the catheter is passing through the optimal port S_1

allowing for the extensibility of the catheter. Figure 4a, b shows the configuration of the catheter as a function of the curvature ζ and τ , while Figure 4c shows the configurations of the catheter as a function of the extension d . In this case, the catheter is constrained at a particular point, which behaves like a transeptal puncture location. Since the catheter is constrained, the catheter bends in the necessary direction to reach a particular point in the orthogonal direction. Figure 4a, b shows a smooth increase in the curvature of the catheter in both possible directions (ζ , τ). In Figure 4c, the catheter is commanded to follow a trajectory along its axis, thereby resulting in an increase in its length. The results show that the model accurately describes the behaviour of the catheter in all three possible degrees of freedom. The experimental validation of the model also confirms that the model accurately predicts the position of sensor 2, considering the position of sensor 1 as the end-effector position and sensor 3 as the base position. The RMS error between the estimated and measured position of sensor 2 is 6.7 mm. The sources of error include misalignment of the sensors along the catheter, sensor noise and the approximation that the curvature of the catheter is the same at all points along the bending section. The simulation and experimental results suggest that the continuum robot model accurately describes the behaviour of the catheter.

In this study we also developed an algorithm to estimate the optimal transeptal puncture location for performing left atrial cardiac ablation. The problem of choosing the location of the transeptal puncture bears similarity to the problem of choosing the ports on the thoracic cavity for insertion of laparoscopic tools and endoscopes to perform robot-assisted minimally invasive surgery (RA-MIS). Several researchers have studied the problem of choosing the optimal ports to maximize the performance of the robot (and surgeon) to perform RA-MIS (26–28). We have implemented the GII to identify the optimal transeptal puncture location to maximize the manoeuvrability of the catheter within the left atrium. The first task was to identify whether the GII is a good measure

for describing the clinician's experience in manoeuvring the catheter. The GII corresponding to the region around the septal wall and the right pulmonary region, regions considered most difficult in which to manoeuvre the catheter, was an order of magnitude less than the overall GII for the entire left atrium. This corroborates closely with the clinician's difficulty in manoeuvring the catheter in this region. The catheter has to bend back on itself to reach the two areas mentioned. This requires a large curvature to be provided to the catheter, which further results in lower singular values of the Jacobian (since the catheter is close to its singular configuration) and a GII value corresponding to poor dexterity.

We also computed the optimal transeptal puncture location by evaluating the location on the septal wall which maximizes the GII. It can be seen from Figure 7b that although the GII corresponding to the point S_1 is larger than that corresponding to S_2 , the condition number at point A is smaller (1.01) for S_2 compared to the condition number of 1.28 for S_1 . This implies that the control of the catheter is more accurate at point A, if S_2 is chosen as the transeptal puncture location. As mentioned earlier, GII is a global measure of the dexterity or isotropy of the catheter at all points in the left atrium, while the condition number is a local measure. Figure 5 shows the result of the computation algorithm. It can be seen that there are certain discrete locations which provide maximum manoeuvrability for the catheter in the left atrium. Since the catheter is constrained to the transeptal puncture point, the catheter loses some dexterity and this can be noticed in the low values of the GII at most points on the septal wall, represented by the red colour in Figure 6a. It should also be noted that the result of the transeptal puncture algorithm is highly specific to the patient and is dependent on the shape and size of the left atrium, position and number of pulmonary veins and the shape and size of the septal wall.

As part of our current work, we are trying to prove the hypothesis that a transeptal puncture location corresponding to a large GII value will lead to better

performance of the clinician. For procedures with a similar level of complexity and for similar shape and size of the heart and pulmonary veins, we will evaluate the correlation between the GII and the amount of manipulation of the catheter (which will be measured as the total distance traveled by the catheter in the left atrium), time taken to complete the procedure from the instant that transseptal puncture is performed and the amount of energy required to ablate the tissue.

As part of our future work, we will register the optimal transseptal puncture location to intracardiac echo images, to help the clinician guide the transseptal needle to the optimal port on the septal wall to obtain maximum dexterity of the catheter in the left atrium.

Conclusion

The objective of this work was to determine the optimal transseptal puncture location and assist the clinician in guiding the needle in real-time to this location. In this study, we have developed an optimization algorithm based on the GII to evaluate the optimal position of the transseptal puncture for left atrial cardiac ablation. As part of this algorithm, we have extended the continuum robot model to describe the kinematics of the catheter within the left atrium. Based on this model, the configuration of the catheter was evaluated such that the catheter makes contact with the desired points on the left atrium, with constraints imposed on its motion by the transseptal puncture. The choice of the transseptal puncture location affects the uniformity of catheter manipulation. The optimal puncture location ensures maximum dexterity of the catheter within the left atrium and also ensures that the catheter has the capability of reaching various locations in the heart. Successful implementation of this algorithm in clinical practice may eventually lead to reducing the time necessary to complete the procedure, improving access to difficult regions in the left atrium, reducing the amount of manipulations of the catheter required to reach a point in the left atrium, and minimizing the amount of fatigue for the clinicians.

Acknowledgement

This research was supported by the Intelligent Surgical Instruments Project, METI Grant, Japan.

References

1. Araf F, Fujimura R, Fukuda T, *et al.* New catheter driving method using linear stepping mechanism for intravascular neurosurgery. In IEEE International Conference on Robotics and Automation, Washington, DC, May 2002; 2944–2949.
2. Tanimoto M, Arai F, Fukuda T, *et al.* Telesurgery system for intravascular neurosurgery. In Medical Image Computing and Computer-Assisted Intervention (MICCAI), 2000; 29–39.
3. Arai F, Tanimoto M, Fukuda T, *et al.* Multimedia telesurgery using high speed optical fiber network and its application to intravascular neurosurgery. In IEEE International Conference on Robotics and Automation, 1996; 878–883.
4. Jayender J, Patel RV, Nikumb S. Robot-assisted active catheter insertion: algorithms and experiments. *Int J Robotics Res* 2009; **28**: 1101–1117.
5. Jayender J, Azizian M, Patel RV. Autonomous robot-assisted image-guided active catheter insertion. *IEEE Trans Robot* 2008; **24**: 858–871.
6. Jayender J, Patel RV. Wave variables based bilateral teleoperation of an active catheter. In IEEE International Conference on Biomedical Robotics and Biomechanics, 2008.
7. Hansen Medical Inc: <http://www.hansenmedical.com/>.
8. Pappone C, Vicedomini G, Manguso F, *et al.* Robotic magnetic navigation for atrial fibrillation ablation. *J Am Coll Cardiol* 2006; **47**: 1390–1400.
9. Ponti RD, Cappato R, Curnis A, *et al.* Trans-septal catheterization in the electrophysiology laboratory: data from a multi-center survey spanning 12 years. *J Am Coll Cardiol* 2006; **47**: 1037–1042.
10. Stocco L, Salcudean SE, Sassani F. Fast constrained global minimax optimization of robot parameters. *Robotica* 1998; **16**: 595–605.
11. Trejos AL, Patel RV, Ross I, *et al.* Optimizing port placement for robot-assisted minimally invasive cardiac surgery. *Int J Med Robotics Comput Assist Surg* 2007; **3**: 355–364.
12. Chirikjian G, Burdick J. A hyper-redundant manipulator. *IEEE Robotics Autom Mag* 1994; **1**: 22–29.
13. Chirikjian GS, Burdick JW. A modal approach to hyper-redundant manipulator kinematics. *IEEE Trans Robotics Autom* 1994; **10**: 343–354.
14. Zanganeh KE, Angeles J. The inverse kinematics of hyper-redundant manipulators using splines. In IEEE International Conference on Robotics and Automation, 1995; 2797–2802.
15. Ebert-Upho I, Chirikjian G. Inverse kinematics of discretely actuated hyper-redundant manipulators using workspace densities. In IEEE International Conference on Robotics and Automation, 1996; 139–145.
16. Mochiyama H, Shimemura E, Kobayashi H. Shape control of manipulators with hyper degrees of freedom. *Int J Robotics Res* 1999; **18**: 584–600.
17. Robinson G, Davies J. Continuum robots – state of the art. In International Conference on Robotics and Automation, 1999; 2849–2854.
18. Bailly Y, Amirat Y. Modeling and control of a hybrid continuum active catheter for aortic aneurysm treatment. In 2005 IEEE International Conference on Robotics and Automation, April 2005; 924–929.
19. Ganji Y, Janabi-Shari F. Kinematic characterization of a cardiac ablation catheter. In IEEE/RSJ International Conference on Intelligent Robots and Systems, 2007; 1876–1881.
20. Mochiyama H, Suzuki T. Kinematics and dynamics of a cable-like hyper-exible manipulator. In IEEE International Conference on Robotics and Automation, 2003; 3672–3677.
21. Tatlicioğlu E, Walker ID, Dawson DM. Dynamic modelling for planar extensible continuum robot manipulators. In IEEE International Conference on Robotics and Automation, 2007; 1357–1362.
22. Sciacivco L, Siciliano B. A solution algorithm to the inverse kinematic problem for redundant manipulators. *IEEE Trans Robotics Autom* 1988; **4**: 403–410.
23. Merlet JP. Jacobian, manipulability, condition number, and accuracy of parallel robots. *J Mech Des* 2006; **128**: 199–206.
24. 3D Slicer: <http://www.slicer.org>.
25. OpenIGTLinkIF: <http://www.namic.org/Wiki/index.php/OpenIGTLink>.
26. Cannon J, Stoll J, Selha S, *et al.* Port placement planning in robot-assisted coronary artery bypass. *IEEE Trans Robotics Autom* 2003; **19**: 912–917.
27. Adhami L, Coste-Maniere E, Coste-Maniere VE, *et al.* Planning and simulation of robotically assisted minimal invasive surgery. In International Conference on Medical Image Computing and Computer Assisted Intervention (MICCAI), 2000; 624–633.
28. Badani KK, Muhletaler F, Fumo M, *et al.* Optimizing robotic renal surgery: the lateral camera port placement technique and current results. *J Endourol* 2008; **22**: 507–510.